#### Research Article

Syed M. Hussain, Rujda Parveen, Nek Muhammad Katbar, Sadique Rehman, Assmaa Abd-Elmonem, Nesreen Sirelkhtam Elmki Abdalla, Hijaz Ahmad, Muhammad Amer Qureshi, Wasim Jamshed\*, Ayesha Amjad, and Rabha W. Ibrahim

# Entropy generation analysis of MHD convection flow of hybrid nanofluid in a wavy enclosure with heat generation and thermal radiation

https://doi.org/10.1515/rams-2024-0037 received January 11, 2024; accepted June 08, 2024

**Abstract:** This work examines the behaviour of flow and heat transmission in the presence of hybrid nanofluid in thermal radiation, heat generation, and magnetohydrodynamics. The hybrid state in this model is represented by two different fluids, TiO<sub>2</sub> (titanium dioxide) and Ag (silver).

\* Corresponding author: Wasim Jamshed, Department of Mathematics, Capital University of Science and Technology (CUST), Islamabad, 44000, Pakistan, e-mail: wasiktk@hotmail.com

Syed M. Hussain: Department of Mathematics, Faculty of Science, Islamic University of Madinah, Madinah, 42351, Saudi Arabia

Rujda Parveen: Department of Mathematics, Dream Institute of Technology, Kolkata, West Bengal, 700104, India

Nek Muhammad Katbar: School of Mathematics and Statistics, Central South University, Changsha, 410083, China; Mehran University of Engineering &Technology SZAB, Campus Khairpur Mir's, Sindh, Pakistan Sadique Rehman: Division of Mathematical and Physical Sciences, Kanazawa University, Kakuma, Kanazawa, 920-1192, Japan

Assmaa Abd-Elmonem, Nesreen Sirelkhtam Elmki Abdalla:

Department of Mathematics, College of Science, King Khalid University,

Abha, Saudi Arabia **Hijaz Ahmad:** Department of Mathematics, Faculty of Science, Islamic University of Madinah, Madinah, 42351, Saudi Arabia; Operational Research Center in Healthcare, Near East University, TRNC Mersin 10, Nicosia, 99138, Turkey; Center for Applied Mathematics and Bioinformatics, Gulf University for Science and Technology, Mishref, Kuwait; Department of Computer Science and Mathematics, Lebanese American University, Beirut, Lebanon

**Muhammad Amer Qureshi:** PYP-Mathematics, College of General Studies, King Fahd University of Petroleum and Minerals, Dhahran, Saudi Arabia; Interdisciplinary Research Center for Hydrogen and Energy Storage, King Fahd University of Petroleum and Minerals, Dhahran, Saudi Arabia

**Ayesha Amjad:** Faculty of Transport and Aviation Engineering, Silesian University of Technology, Gliwice, Poland

**Rabha W. Ibrahim:** Faculty of Engineering and Natural Sciences, Advanced Computing Lab, Istanbul Okan University, Turkey; Information and Communication Technology Research Group, Scientific Research Center, Al-Ayen University, Thi-Qar, Iraq The enclosure is wavy and slanted, with curving walls on the left and right. The finite difference approximation method was utilized to resolve the fundamental equations after they were non-dimensionalized, which are further reduced to a fourth-order bi-harmonic equation and are numerically solved based on the biconjugate gradient-stabilized approach method. The simulations are performed with various Rayleigh numbers, Hartmann numbers, an inclination angle of the enclosure, radiation parameters, heat generation parameters, inclination angle of the magnetic field, and volume fraction of hybrid nanoparticles. The streamlines, isotherms, and average Nusselt number contours are used to depict the thermo-fluid patterns. The findings show that the average Nusselt number relies on  $\phi$ and increases as  $\phi$  rises. The investigation's findings demonstrated that the transfer of heat on the heated bottom wall significantly increases with the Rayleigh number ( $Ra = 10^5$ and 10<sup>6</sup>). At a cavity inclination of 45°, interesting multivortex structures are observed. The results of this study may enhance the effectiveness of solar collectors, heat exchangers, and other similar systems that depend on convective heat transfer in nature.

**Keywords:** hybrid nanofluid, inclined wavy enclosure, MHD, thermal radiation, biconjugate gradient-stabilized method

#### Nomenclature

- x, y distance along x and y coordinate, m
- X, Y non-dimension distance along the x and y
  - coordinate
- u, v x and y components of velocity
- U, V x and y components of dimensionless velocity
- T temperature of the fluid (K)
- P pressure (Pa)
- P non-dimension pressure
- Pr Prandtl number

2 — Syed M. Hussain et al. DE GRUYTER

$C_{ m p}$	specific heat at constant pressure (J·kg <sup>-1</sup> ·K <sup>-1</sup> )
$B_o$	magnetic field strength (T)
На	Hartmann number
а	amplitude of the side-curved walls
$\boldsymbol{G}$	acceleration due to gravity (m·s <sup>-2</sup> )
k	thermal conductivity (Wm <sup>-1</sup> ·K <sup>-1</sup> )
$Q_0$	heat generation parameter
$q_{ m r}$	radiative heat flux
Nu <sub>avg</sub>	average Nusselt number
Ra	Rayleigh number
Rd	radiation parameter
$S_{ m loc}$	local entropy generation
$\mathcal{S}_{ heta}$	non-dimension entropy generation due to heat
	transfer
$\mathcal{S}_{\psi}$	non-dimension entropy generation due to fluid
	friction
$S_m$	dimensionless entropy generation due to mag-
	netic field
α	thermal diffusivity (m <sup>2</sup> ·s <sup>-1</sup> )
β	thermal expansion coefficient
γ	inclination angle of magnetic field
δ	inclination angle of the enclosure
$\phi$	volume fraction of nanoparticles
ω	dimensionless vorticity
$\theta$	temperature
σ	electrical conductivity (Ωm)
μ	dynamic viscosity (Wm <sup>-1</sup> ·K <sup>-1</sup> )
$\psi$	non-dimensional stream function
ν	kinematic viscosity (m <sup>2</sup> ·s <sup>-1</sup> )

#### 1 Introduction

Many industrial-based fluid flow problems were the target of obtaining better heat distribution and energy loss control to make their process optimal. The particular choice of fluid in the system becomes vital. Base fluids such as water and ethylene glycol were employed in the early stages. After the arrival of a better nanofluid with higher thermal efficiency, significant improvements were noted in the application of heat transfer. Nanofluids have greater thermal conductivities than base fluids since they are made of suspended nanoparticles in traditional fluids, e.g., ethylene glycol, oil, and water. Researchers have been giving the term "nanofluid" a lot of thought ever since Choi and Eastman [1] coined it. The primary applications and underlying models for the study of nanofluids were reported by Tiwari and Das [2] and Buongiorno [3]. With additional study, specifically designed nanofluids may prove essential for effectively transferring

heat in natural convection scenarios over various geometries [4–7].

Advanced nanofluids known as hybrids are said to possess even superior thermal characteristics than conventional nanofluids. Nanoparticles of two or more different materials, either the same size or different, are combined with a conventional fluid to create hybrid nanofluids. Hybrid nanofluids are more economically viable and essential for industry due to their superior performance over nanofluids. This fact inspired numerous researchers, who examined the characteristics of hybrid nanoliquids under various conditions [8-12]. Three-dimensional natural convection and entropy formation in a trapezoidal cavity with wavy walls were studied by Al-Kouz et al. [13] using an electrically conducting water-CNT/Fe<sub>3</sub>O<sub>4</sub> hybrid nanofluid. The findings demonstrated that for very high Hartmann and high Rayleigh numbers, the average Nusselt number is much reduced. Heat and mass transfer via a biaxial stretching sheet with anisotropic slip and entropy/Bejan on a three-dimensional boundary-layer hybrid nanofluid was studied by Ahmed et al. [14].

The flow of a fluid (such as a liquid or a gas) inside a container or enclosure is referred to as the flow in a cavity. The flow within an enclosure has been intensively explored in the dynamics of fluids. The examination of flow inside an enclosed cavity has multiple applications, such as in the area of engineering, in understanding the behaviour of fluids in natural systems, and in the creation of technologies that depend on the manipulation of fluids. The numerical investigation of the coupled natural convection flow outside and inside of an enclosed cylindrical chamber that is embedded with an internal source of heat was conducted by Zhang et al. [15]. In a novel geometry, a triangular cavity having a pentagonal obstruction, Hosseinzadeh et al. [16] investigated the mixed convection flow of thermal transport by employing the finite element method. As per their findings, a rise in the buoyancy ratio parameter causes a considerable increase in the isotherm profile that surrounds the pentagonal obstacle of the enclosure. The study conducted by Hossain et al. [21] involved the study of heat transmission and entropy formation of magnetic nanofluids inside a square chamber that contained carbon nanotubes. To investigate the fluid properties, Roshani et al. [18] took into consideration two octagonal cavities with horizontal and vertical Cassini oval barriers along with specific boundary conditions. Using the quadratic Boussinesq approximation, Salawu et al. [19] have explored the entropy generation and current density of electromagnetic tangent hyperbolic hybridized nanofluids inside a thermal convective cooling channel. The fluid flow properties and the efficiency of heat transfer inside wavy enclosures have been the subject of recent studies [20–23].

Despite having significant applications in real-world issues like placing solar collectors to capture the most solar energy possible and many more, there is not much research on geometric inclination angles in the literature. Nabwey et al. [24] investigated the influence of geometric preference angle on the heat transfer amount in a U-shaped cavity by considering heat generation and absorption. Adopting the Darcy-Brinkman-Forchheimer theory, Keerthi Reddy et al. [25] examined the liquid flow dynamics in the porous annular area. They discovered that altering the geometric tilt angle changed the convective strength inside the container. Moolya and Satheesh [26] looked at how the magnetic field and cavity inclination angle affected the movement of mass and heat transfer. The findings demonstrated that when the cavity and magnetic field inclination angles are increased, convective heat and mass transfer increase as well. For the case of the magnetic field effect produced by the Lorentz force, an opposite trend is observed.

Bakar *et al.* [27] considered the assorted convection with a mixture of nanofluids in a porous medium subjected to magnetohydrodynamics (MHD), suction/injection, radiation, and heat generation. The mixed convective flow of Casson MHD hybrid nanofluid on a surface using the Buongiorno ideal along dissipative possessions has been extensively studied by Algehyne *et al.* [28]. They claimed that the velocity distribution is reduced with an appreciation of the magnetic effect. Yasmin *et al.* [29] discussed the mixed convection and thermal radiation flow due to a stretched cylinder containing microorganisms in the presence of cross nanofluid. Utilizing the Cattaneo–Christov heat and mass flux model, Yasmin *et al.* [30] examined the three-

dimensional electro-MHD Cu-Al<sub>2</sub>O<sub>3</sub>/water hybrid nanofluid flow on a Riga plate. According to the data, there is a positive correlation between the radiation factor and the Nusselt number. Aghakhani et al. [31] examined the implications of radiation and magnetic fields on the convective heat transfer and entropy production of a nanofluid inside a slant zone. By increasing Ra from 10<sup>3</sup> to 10<sup>5</sup>, they revealed that the supreme entropy and heat transfer rate reinforced 3.77 and 2.69 times, respectively. To investigate the convection flow, Mohammadi and Gandjalikhan Nassab [32] took into account the Soret and Dufour phenomena in a complex geometry under the radiation effect. They discovered that altering the Dufour (Soret) parameter value would influence the mass (heat) transfer, based on its value. A numerical study of various convections in the presence of heat generation internally in a hollow-containing nanofluid was provided by Yu et al. [33].

Following the review of the literature, it is noted that there are enough studies on the cavity problem that take into account the magnetic field, buoyancy force, and nanofluid with various boundary conditions. The combined effects of heat generation, thermal radiation, and magnetic field on free convection phenomena in an inclined geometry saturated with hybrid nanofluid, however, have not been thoroughly studied. The current study is a modest attempt to bridge this research gap and discover new physics. This study examines the flow, heat, and production of entropy in an inclined enclosure containing hybrid nanofluid, taking into account several parameters, including the enclosure inclination angle ( $\delta$ ), Hartmann number (Ha), magnetic field inclination angle ( $\gamma$ ), Rayleigh number (Ra), heat generation ( $Q_0$ ), and thermal radiation (Rd).

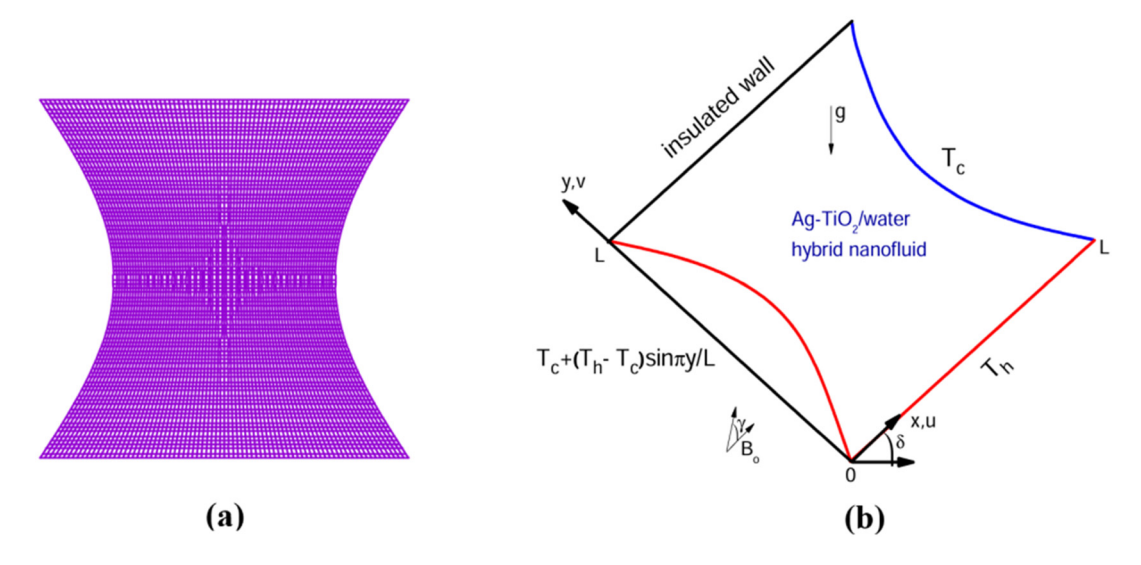


Figure 1: (a) Mesh of the cavity and (b) schematic representation of the physical domain featuring several wall boundary conditions.

# 2 Methodology

#### 2.1 Model description

Figure 1 describes the physical and schematic configuration for studying the convection. This is a 2D inclined enclosure that is exposed to different thermal boundary conditions and filled with  $Ag/TiO_2$  hybrid nanofluid. The lower wall is at temperature  $T_{\rm h}$ , the sinusoidally heated left wall, the temperature of the right wall is at  $T_{\rm c}$  with  $T_{\rm c} < T_{\rm h}$ , while the top wall is thermally isolated. The enclosure experiences convection flow as a result of the temperature variation at the walls.

The Boussinesq estimate is approved for the statistical frame. The fluid used in this analysis is thought to have laminar flow, be Newtonian, and be incompressible. The induced magnetic field and viscous dissipation are ignored, while the radiative heat flux is considered in the present analysis.

## 2.2 Governing equations

The equations governing the Boussinesq approximation for hybrid nanofluids [34,35] in the dimensional form are represented below:

Continuity equation:

$$\frac{\partial u}{\partial x} + \frac{\partial v}{\partial y} = 0.$$
(1)

Momentum conservation equations:

$$u\frac{\partial u}{\partial x} + v\frac{\partial u}{\partial y} = -\frac{1}{\rho_{\rm hnf}}\frac{\partial p}{\partial x} + v_{\rm hnf}\left[\frac{\partial^2 u}{\partial x^2} + \frac{\partial^2 u}{\partial y^2}\right] + g_1, \quad (2)$$

$$u\frac{\partial v}{\partial x} + v\frac{\partial v}{\partial y} = -\frac{1}{\rho_{\rm hnf}}\frac{\partial p}{\partial y} + v_{\rm hnf}\left[\frac{\partial^2 v}{\partial x^2} + \frac{\partial^2 v}{\partial y^2}\right] + g_2. \quad (3)$$

Energy equation:

$$u\frac{\partial T}{\partial x} + v\frac{\partial T}{\partial y} = \alpha_{\rm hnf} \left[ \frac{\partial^2 T}{\partial x^2} + \frac{\partial^2 T}{\partial y^2} \right] - \frac{1}{(\rho C_{\rm p})_{\rm hnf}} \left[ \frac{\partial q_{\rm rx}}{\partial x} + \frac{\partial q_{\rm ry}}{\partial y} \right] + \frac{q_o}{(\rho C_{\rm p})_{\rm hnf}} (T - T_c),$$
(4)

where

$$g_1 = \frac{g(\rho\beta)_{\text{hnf}}}{\rho_{\text{hnf}}} (T - T_c) \sin\delta + \frac{\sigma_{\text{hnf}}}{\rho_{\text{hnf}}} B_0^2 (\nu \sin\gamma \cos\gamma - u \sin^2\gamma),$$

$$g_2 = \frac{g(\rho\beta)_{\text{hnf}}}{\rho_{\text{hnf}}} (T - T_c)\cos\delta + \frac{\sigma_{\text{hnf}}}{\rho_{\text{hnf}}} B_0^2(u\sin\gamma\cos\gamma - v\cos^2\gamma).$$

The Rosseland diffusion approximation for heat fluxes due to radiation along x and y directions are given by

$$q_{\rm rx} = \frac{-4}{3} \frac{\sigma_{\rm e}}{\beta_{\rm p}} \frac{\partial T^4}{\partial x}$$
 and  $q_{\rm ry} = \frac{-4}{3} \frac{\sigma_{e}}{\beta_{\rm p}} \frac{\partial T^4}{\partial y} [T^4 \cong 4T_c^3 T - 3T_c^4].$ 

Table 1 provides the thermophysical features of Ag and TiO<sub>2</sub>, and the features of the studied nanofluid are assessed in the following manner:

Effective density:

$$(\rho_{\rm hnf}) = (1 - \phi)\rho_{\rm f} + \phi_{1}\rho_{1} + \phi_{2}\rho_{2}.$$

Specific heat capacitance:

$$(\rho c_{\rm p})_{\rm hnf} = (1 - \phi)(\rho C_{\rm p})_{\rm f} + \phi_1(\rho C_{\rm p})_1 + \phi_2(\rho C_{\rm p})_2$$

Thermal expansion coefficient:

$$(\rho\beta)_{hnf} = (1 - \phi)(\rho\beta)_f + \phi_1(\rho\beta)_1 + \phi_2(\rho\beta)_2.$$

Effective thermal conductivity:

$$k_{\rm hnf} = k_{\rm f} \left[ \frac{\frac{\phi_1 k_1 + \phi_2 k_2}{\phi} + 2k_{\rm f} + 2(\phi_1 k_1 + \phi_2 k_2) - 2(\phi_1 + \phi_2) k_{\rm f}}{\frac{\phi_1 k_1 + \phi_2 k_2}{\phi} + 2k_{\rm f} - (\phi_1 k_1 + \phi_2 k_2) + (\phi_1 + \phi_2) k_{\rm f}} \right].$$

Thermal diffusivity:

$$\alpha_{\rm hnf} = \frac{k_{\rm hnf}}{(\rho C_{\rm p})_{\rm hnf}}.$$

Effective dynamic viscosity:

$$\mu_{\rm hnf} = \mu_{\rm f} (1 - \phi_1 - \phi_2)^{-2.5}$$
.

Electrical conductivity:

$$\sigma_{\rm hnf} = \sigma_{\rm f} \left[ 1 + \frac{3(\zeta - \phi)}{\left[ \frac{\zeta}{\phi} + 2 \right] - (\zeta - \phi)} \right].$$

At this point,  $\phi(=\phi_1+\phi_2)$  characterizes the hybrid nanoparticle capacity fraction of and  $\zeta=\frac{\phi_1\sigma_1+\phi_2\sigma_2}{\sigma_2}$ . The

Table 1: Thermophysical features of water, Aq, and TiO<sub>2</sub> [27]

Physical properties	Pure water	Ag	TiO <sub>2</sub>
$C_p$ (J·kg <sup>-1</sup> ·K <sup>-1</sup> )	4,179	235	686
$\rho$ (kg·m <sup>-3</sup> )	997.1	10,500	4,250
$k \text{ (Wm}^{-1} \cdot \text{K}^{-1})$	0.613	429	8.9538
$\beta \times 10^5 \text{ (1·K}^{-1}\text{)}$	21	1.89	0.9

subscripts f, 1, and 2 are utilized to mention the immoral fluid, Ag nanoparticles, and  $TiO_2$  nanoparticles correspondingly.

The governing equations in the nondimensional form are as follows:

$$\frac{\partial U}{\partial X} + \frac{\partial V}{\partial Y} = 0, \tag{5}$$

$$U\frac{\partial U}{\partial X} + V\frac{\partial U}{\partial Y} = -\frac{\partial P}{\partial X} + \frac{\mu_{\text{hnf}}}{\rho_{\text{hnf}}\alpha_{\text{f}}} \left[ \frac{\partial^2 U}{\partial X^2} + \frac{\partial^2 U}{\partial Y^2} \right] + G_1, \quad (6)$$

$$U\frac{\partial V}{\partial X} + V\frac{\partial V}{\partial Y} = -\frac{\partial P}{\partial Y} + \frac{\mu_{\rm hnf}}{\rho_{\rm hnf}\alpha_{\rm f}} \left[ \frac{\partial^2 V}{\partial X^2} + \frac{\partial^2 V}{\partial Y^2} \right] + G_2, \quad (7)$$

$$U\frac{\partial \theta}{\partial X} + V\frac{\partial \theta}{\partial Y} = \left[\frac{\alpha_{\rm hnf}}{\alpha_{\rm f}} + \frac{4}{3} \frac{(k_{\rm hnf}/k_{\rm f})}{(\rho C_{\rm p_{hnf}}/\rho C_{\rm p_{\rm f}})} \left[\frac{k_{\rm hnf}}{k_{\rm f}}\right]^{-1} \operatorname{Rd} \left[\frac{\partial^{2} \theta}{\partial X^{2}} + \frac{\partial^{2} \theta}{\partial Y^{2}}\right] + \frac{\alpha_{\rm hnf}}{\alpha_{\rm f}} Q_{o} \theta,$$
(8)

where

$$G_{1} = \frac{(\rho \beta_{s})_{hnf}}{\rho_{hnf} \beta_{f}} \text{ Ra Pr } \theta \sin \delta + \frac{\sigma_{hnf} \rho_{f}}{\sigma_{f} \rho_{hnf}} \text{Ha}^{2} \text{Pr}(V \sin y \cos y)$$
$$- U \sin^{2} v).$$

$$G_2 = \frac{(\rho \beta_s)_{hnf}}{\rho_{hnf}\beta_f} \text{Ra Pr } \theta \cos \delta + \frac{\sigma_{hnf}\rho_f}{\sigma_f \rho_{hnf}} \text{Ha}^2 \text{Pr}(U \sin y \cos y)$$
$$- V \cos^2 y).$$

The dimensionless parameters, *i.e.*, Rayleigh number (Ra), Hartmann number (Ha), Prandtl number (Pr), and radiation parameter (Rd), are, respectively, defined as follows:

$$\begin{aligned} & \text{Pr} = \frac{v_{\text{f}}}{a_{\text{f}}}, \; \text{Ra} = \frac{g\beta_{\text{f}}(T_{\text{h}} - T_{\text{c}})L^{3}}{v_{\text{f}}a_{\text{f}}}, \; \text{Ha} = \sqrt{\frac{\sigma_{\text{f}}}{\mu_{\text{f}}}}B_{0}L, \; \text{Rd} = \frac{4T_{\text{c}}^{3}}{k_{\text{f}}}\frac{\sigma_{\text{e}}}{\beta_{\text{R}}}, \\ & \text{and} \; q_{o} = \frac{Q_{o}L^{2}}{(\rho c_{\text{p}})_{\text{hnf}}a_{\text{hnf}}}. \end{aligned}$$

## 2.3 Boundary conditions

In the non-dimensional structure, boundary requirements include:

all walls, U = 0, and V = 0

At the left-curved wall:  $\theta = \sin \pi Y$ ,

At the right-curved wall:  $\theta = 0$ ,

At the bottom wall:  $\theta = 1$ ,

At the top wall:  $\frac{\partial \theta}{\partial V} = 0$ .

The Nusselt number, Nu, is the measure of the convective heat transfer coefficient at the hot surface. The higher the value of Nu, the higher the rate of heat transfer from the surface.

The local Nusselt number at the bottom wall is computed as follows:

$$Nu = -\frac{k_{\text{hnf}}}{k_{\text{f}}} \frac{\partial \theta}{\partial Y} + \frac{4}{3} \text{Rd} \frac{\partial \theta}{\partial Y}.$$
 (9)

The average Nusselt number (Nu<sub>avg</sub>) is obtained by integrating the local Nusselt number (Nu) along the respective wall. The dimensionless local entropy generation due to heat transfer  $(S_{\theta})$ , due to fluid friction  $(S_{\psi})$ , and due to the magnetic field  $(S_m)$  for a 2-D fluid flow and heat in the Cartesian coordinate can be written as

$$S_{\theta} = \frac{k_{\text{hnf}}}{k_{\text{f}}} \left[ \left( \frac{\partial \theta}{\partial X} \right)^{2} + \left( \frac{\partial \theta}{\partial Y} \right)^{2} \right], \tag{10}$$

$$S_{\psi} = \lambda \frac{\mu_{\text{hnf}}}{\mu_{\text{f}}} \left[ 2 \left[ \left( \frac{\partial U}{\partial X} \right)^2 + \left( \frac{\partial V}{\partial Y} \right)^2 \right] + \left( \frac{\partial U}{\partial Y} + \frac{\partial V}{\partial X} \right)^2 \right], \quad (11)$$

$$S_m = \lambda \frac{\sigma_{\text{hnf}}}{\sigma_{\text{f}}} \text{Ha}^2 (U \sin \gamma - V \cos \gamma)^2, \tag{12}$$

where  $\lambda$  is the irreversibility ratio, defined as

$$\lambda = \frac{\mu_{\rm f} T_0}{k_{\rm f}} \left( \frac{\alpha}{L \Delta T} \right)^2,\tag{13}$$

where  $\mu$  and k are the dynamic viscosity and thermal conductivity of the fluid, respectively. Here, we have considered  $\lambda$  as  $10^{-4}$  [36].

The local entropy generation  $S_{loc}$  can be written as

$$S_{\text{loc}} = S_{\theta} + S_{\psi} + S_{m}. \tag{14}$$

The summation of total entropy generation due to fluid friction, heat transfer, and magnetic field gives the total entropy production and is given as

$$S_{\text{total}} = S_{\theta,t} + S_{\psi,t} + S_{m,t},$$
 (15)

where

$$S_{\theta,t} = \int_{V} S_{\theta} dV, \quad S_{\psi,t} = \int_{V} S_{\psi} dV, \quad S_{m,t} = \int_{V} S_{m} dV.$$

# 3 Methodology

The biconjugate gradient-stabilized approach, commonly referred to as Bi-CGStab in numerical linear algebra, is an adaptive methodology created by Van der Vorst for the numerical explanation of nonsymmetric linear equations. It is a variation of the biconjugate gradient process (BiCG), and compared to other variations such as the conjugate gradient-squared (CGS) method, it converges more quickly and smoothly. A Krylov subspace approach is used. It does not call for multiplication by the transpose of the system matrix, in contrast to the original BiCG approach.

The vorticity  $(\omega)$  and stream function  $(\psi)$  in the non-dimensional formula are assumed *via*:

$$U = \frac{\partial \psi}{\partial Y}, \ V = -\frac{\partial \psi}{\partial X}, \ \text{and} \ \omega = \frac{\partial V}{\partial X} - \frac{\partial U}{\partial Y},$$
 (16)

which gives a single equation

$$\frac{\partial^2 \psi}{\partial X^2} + \frac{\partial^2 \psi}{\partial Y^2} = -\omega. \tag{17}$$

The negative sign of  $\psi$  represents the clockwise circulations, while the positive value of  $\psi$  represents the anticlockwise circulations. Stream function contours provide a basic model of nanofluid flow and are highly helpful in the determination of flow potential (Figure 2).

Utilizing equation (16) and removing pressure term from equations (6) and (7), we obtain

$$\frac{\mu_{\text{hnf}}}{\rho_{\text{hnf}}} \alpha_{\text{f}} \left( \frac{\partial^{2} \omega}{\partial X^{2}} + \frac{\partial^{2} \omega}{\partial Y^{2}} \right) - \left( U \frac{\partial \omega}{\partial X} + V \frac{\partial \omega}{\partial Y} \right) 
- \frac{(\rho \beta)_{\text{hnf}}}{\rho_{\text{hnf}}} \text{Ra} \Pr \left[ \left( \frac{\partial \theta}{\partial Y} \sin \delta - \frac{\partial \theta}{\partial X} \cos \delta \right) \right] 
- \frac{\sigma_{\text{hnf}} \rho_{\text{f}}}{\sigma_{\text{f}} \rho_{\text{hnf}}} \text{Ha}^{2} \Pr \left( \frac{\partial V}{\partial Y} \sin y \cos y - \frac{\partial U}{\partial Y} \sin^{2} y \right) 
- \frac{\partial U}{\partial X} \sin y \cos y + \frac{\partial V}{\partial V} \cos^{2} y \right] = 0.$$
(18)

Curve boundary implementation on rectangular grids is challenging when curved walls are present. As a result, the regular (square) computational aspects domain  $(\xi, \eta)$  is created from the fluid domian (X, Y). In this effort, we have reflected the succeeding coordinate alteration:

$$\xi = \frac{X - F_1(Y)}{F_2(Y) - F_1(Y)}$$
 and  $\eta = Y$ ,

where  $F_1(Y) = \sin \pi \eta$  and  $F_2(Y) = 1 - \sin \pi \eta$ 

The governing equations can be assessed in  $\xi - \eta$  domain utilizing the succeeding association:

where

$$J = \frac{\partial(X, Y)}{\partial(\xi, \eta)} = \begin{vmatrix} \frac{\partial X}{\partial \xi} & \frac{\partial X}{\partial \eta} \\ \frac{\partial Y}{\partial \xi} & \frac{\partial Y}{\partial \eta} \end{vmatrix}$$

is the Jacobian of the transformation.

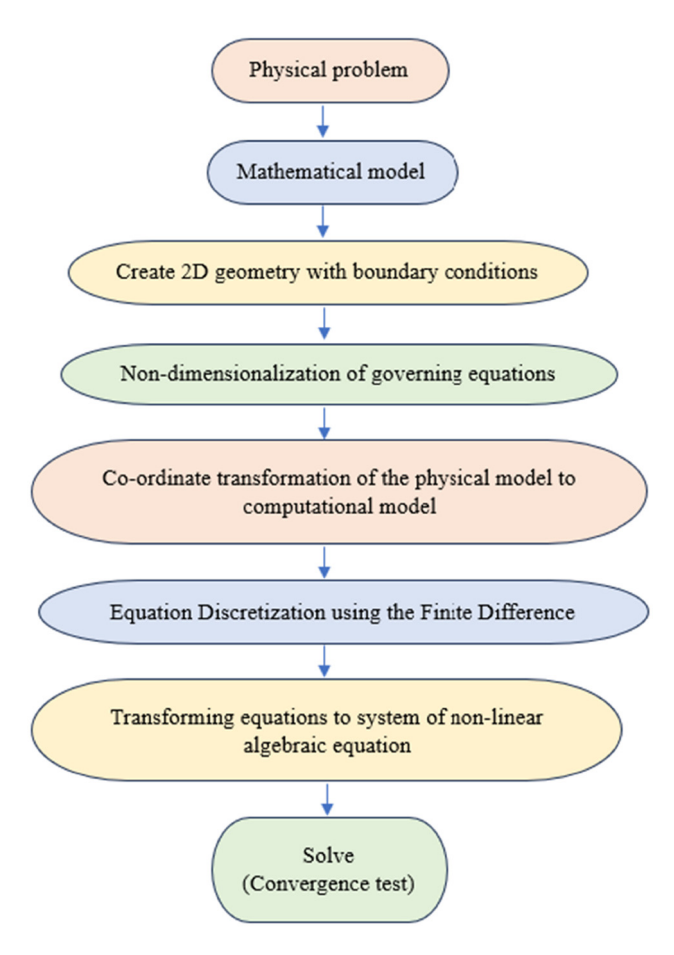


Figure 2: Flowchart to solve the considered problem.

The second-order central difference discretization is applied to the transformed governing equations and inscribed in matrix procedure equally:

$$A\psi = f \left[ \text{Ra, Pr, Ha, } U, V, \frac{\partial \theta}{\partial \xi}, \frac{\partial \theta}{\partial \eta}, \frac{\partial \psi}{\partial \xi}, \frac{\partial \psi}{\partial \eta} \right], (19)$$

$$B\theta = 0. \tag{20}$$

where A and B are the coefficient matrices of order mn. The resulting nonlinear algebraic equations (19) and (20) are resolved to use the outer–inner repetition technique, BiCGStab method. The detailed procedure and application of the method are given in Parveen  $et\ al.\ [37,38]$ . The numerical process is realized in Fortran software. The convergence is achieved when the relative error for each variable  $(\psi\ and\ \theta)$  satisfies the convergence criterion  $(0.5\times 10^{-6})$ .

A test for grid independence is conducted under the circumstances of Ra =  $10^3$ , Ha = 20,  $\delta = 45^0$ , and  $\phi = 0.02$  for  $\psi_{\min}$  for different grid sizes  $21 \times 21$ ,  $41 \times 41$ ,  $81 \times 81$ , and  $161 \times 161$ . The outputs of the grid test are represented in

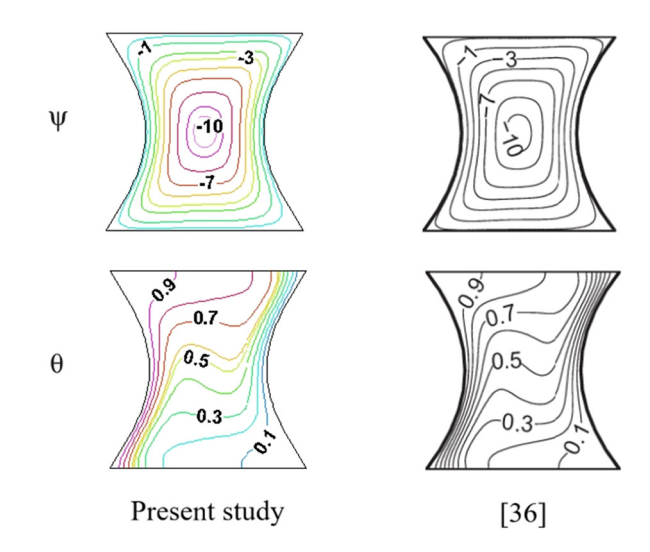
**Table 2:** Grid independence test for  $\psi_{\rm min}$  at Ra =  $10^3$ , Ha = 20, Rd =  $1, \delta = 45^\circ$ ,  $\gamma = 30^\circ$ ,  $\gamma = 20^\circ$ , and  $\gamma = 20^\circ$ , and

	21 × 21	41 × 41	81 × 81	161 × 161
$\psi_{ m min}$	-0.0623	-0.0619	-0.0614	-0.0612

**Table 3:** Comparison of the existing investigation through the former effort of Ece and Büyük [39] for  $\psi_{\min}$  for various inclination angles of the enclosure ( $\delta$ ) and Hartmann number (Ha) at Grashof number =  $10^5$ 

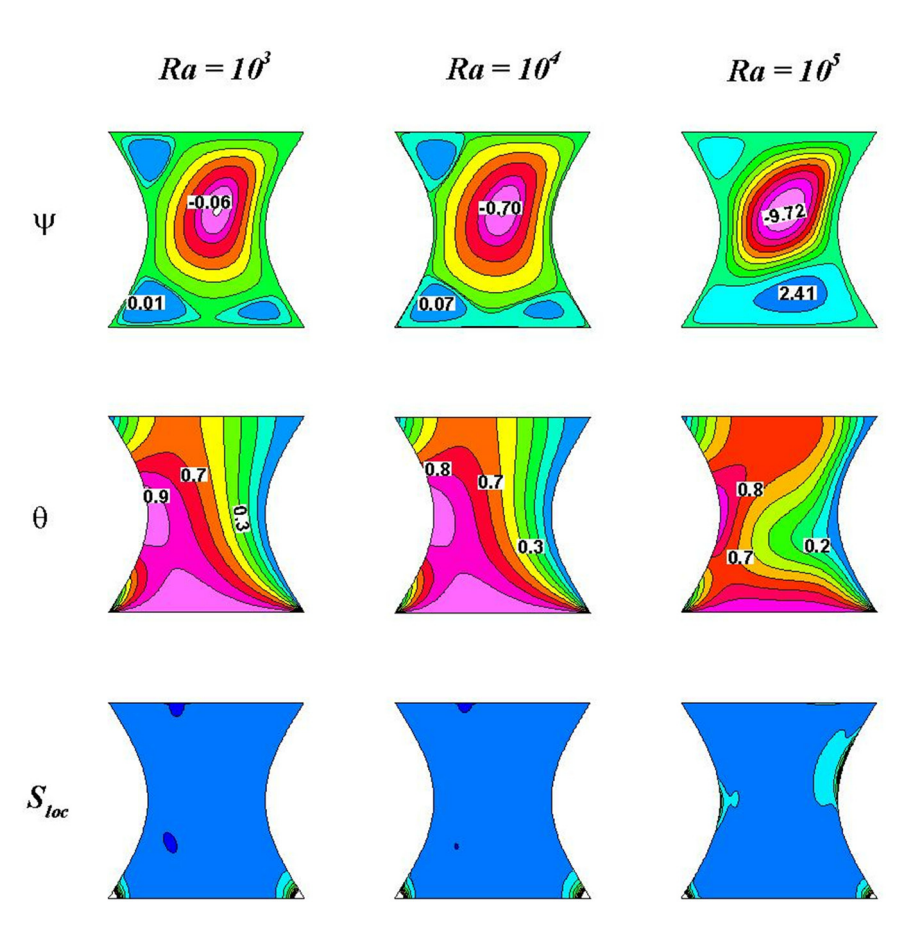
	δ	-45°	0°	45°
Ha = 0	[39]	-13.0627	-20.3580	-11.4623
	Present	-13.0714	-20.3760	-11.4792
Ha = 100	[39]	-1.4059	-1.4958	-0.5086
	Present	-1.4046	-1.4956	-0.5087

Table 2. As can be seen in Table 2, the grid sizes  $81 \times 81$  and higher show consistent results of  $\psi_{\min}$ . As a result, an  $81 \times 81$  grid size is taken throughout the computational purpose.



**Figure 3:** Comparison of the current work through the previous information of Biswal and Basak [36] for streamlines and isotherms for at Pr = 1,000 and  $Ra = 10^5$ .

Authentication of the numerical scheme employed in this work was verified through the comparative analysis of



**Figure 4:** Flow pattern, isotherms, and local entropy production for various Rayleigh numbers (Ra) at Ha = 20, Rd = 1,  $Q_0$  = 5,  $\delta$  = 45°,  $\gamma$  = 30°, and  $\phi$  = 0.02.

8 — Syed M. Hussain et al. DE GRUYTER

the Hartmann number (Ha) and inclination angle ( $\delta$ ) with the existing results of Ece and Büyük [39]. The results are presented in Table 3. To confirm the certification and perform a double check, the isotherms, and streamlines with Biswal and Basak [36] for curved enclosure with cold right wall and hot left wall at Pr = 1,000 and Ra =  $10^5$  (Figure 3). In both cases, it seems to have good coherence, and with that confidence, the results for entropy and thermal aspects were obtained and exhibited in the form of flow patterns, isotherms, Nusselt, and entropy displays.

numerically. Plots and tables are utilized to assess the results of this study. The considered dimensionless parameters are Rayleigh number (Ra =  $10^3 - 10^5$ ), Hartmann number (Ha = 0-60), the inclination angle of the cavity ( $\delta = 0-90^\circ$ ), magnetic field inclination angle ( $\gamma = 0-90^\circ$ ), heat generation ( $\gamma = 0-10$ ), thermal radiation (Rd =  $\gamma = 0-20$ ), and volume fraction of nanoparticles ( $\gamma = 0-0.06$ ). The Prandtl number is taken as  $\gamma = 6.2$  for the study. To analyse the heat transport rate, the average Nusselt number ( $\gamma = 0.000$ ) is determined.

### 4 Results and discussions

This investigation presents the impacts of heat generation, thermal radiation, and magnetic fields on the temperature fields, flow, and entropy production of a hybrid nanofluid inside a squeezed-shaped container. The finite difference approach is utilized to analyse the fundamental equations

#### 4.1 Significance of Rayleigh number (Ra)

Figure 4 represents the inspiration of Rayleigh number (Ra) on streamlines, isotherms, and entropy generation. As depicted in this figure, at  $Ra = 10^3$ , one primary clockwise rotating vortex is formed that fills the entire cavity showing conduction dominant inside the enclosure. With escalating Ra, a small anticlockwise vortex appeared at the bottom share of the enclosure. This happens due to grow in

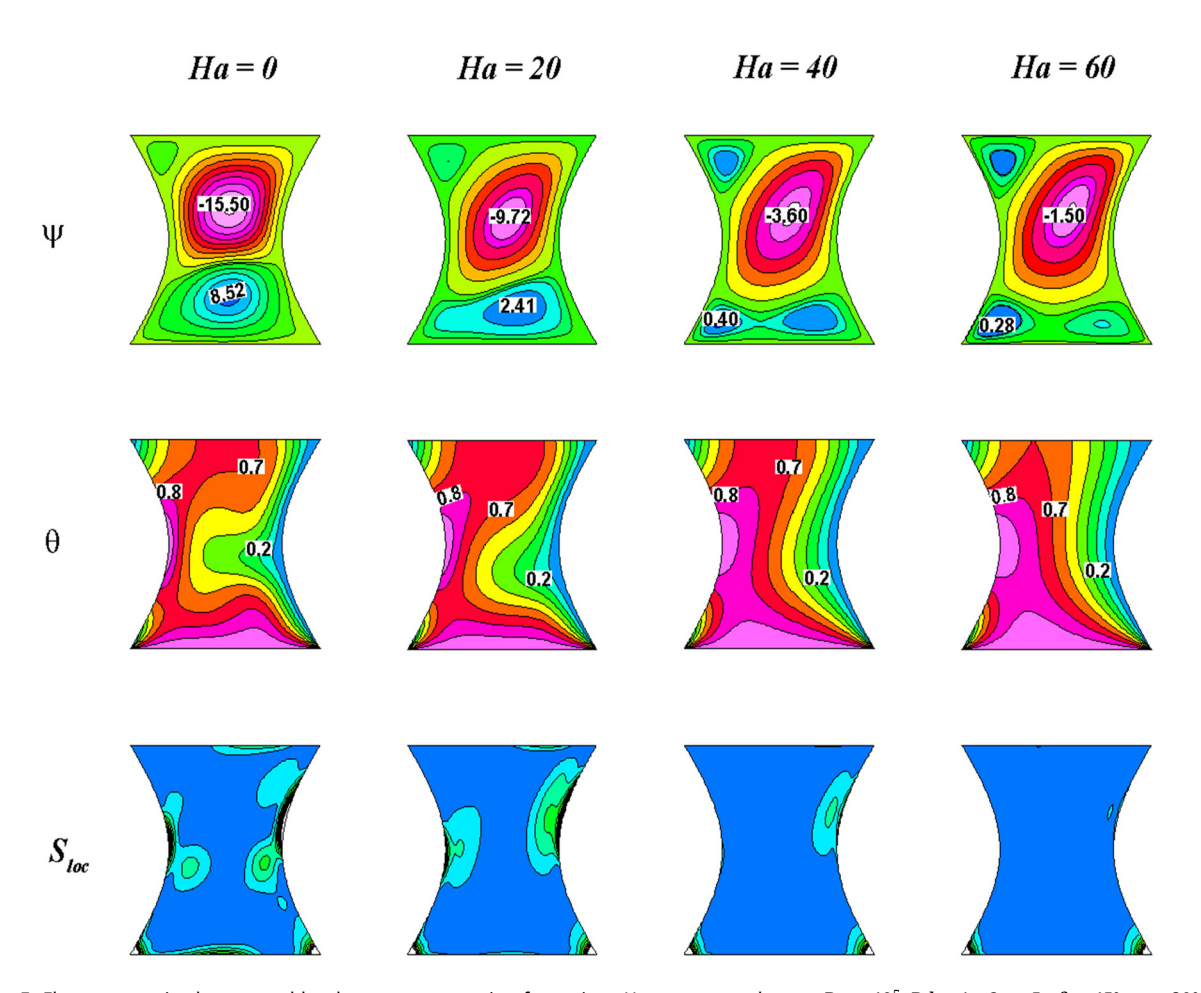


**Figure 5:** Flow pattern, isotherms, and local entropy generation for various Hartmann numbers at Ra =  $10^5$ , Rd = 1,  $Q_0$  = 5,  $\delta$  =  $45^\circ$ ,  $\gamma$  =  $30^\circ$ , and  $\phi$  = 0.02.

buoyancy forces with the increase in Ra that leads to intensified fluid velocity as well as the convection effect. The isotherm pattern becomes stratified with the increase in Ra. The primary heat transfer method within the enclosure is conduction, which changes into convection when Ra rises. Also, with an increase in the temperature distribution, the entropy generation increases, which leads to a uniform distribution of entropy generation inside the cavity.

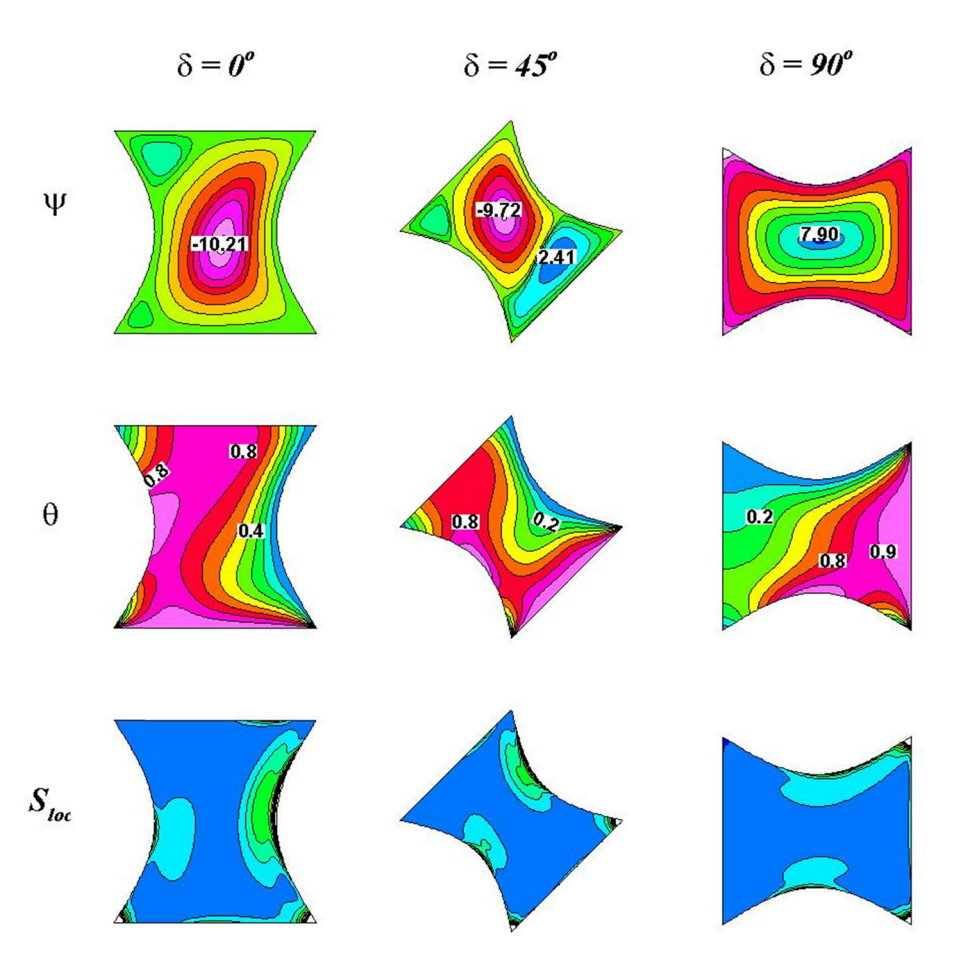
## 4.2 Significance of Hartmann number (Ha)

Figure 5 displays the flow pattern, thermal pattern, and entropy production for various ranges of Hartmann number (Ha) at Ra =  $10^5$ ,  $\delta = 45^\circ$ ,  $\gamma = 30^\circ$ , Rd = 1,  $Q_0 = 5$ , and  $\phi = 0.02$ . From the flow lines, it is found that the upper part of the enclosure has primary clockwise vortices and the lower part of the enclosure has secondary anti-clockwise vortices when there is no magnetic field, *i.e.*, at Ha = 0. As the value of Ha rises, the primary clockwise vortices enlarges

and the secondary vortices at the lower part of the enclosure begins to deteriorate due to the presence of Lorentz force, which is the consequence of magnetic field. This signifies that the strength of convective cells decreases. As shown in Figure 6, the stream function value decreases from  $\psi_{\rm min}$ = –15.654 for Ha = 0 to  $\psi_{\rm min}$ = –1.510 for Ha = 60. The isotherm bentness within the enclosure attenuates with rising values of Ha. This shows that the conduction heat transfer dominates over convection heat transfer as Ha rises. Maximum entropy generation takes place at the bottom wall's corners, whereas as the magnetic factor rises, the entropy loss gets reduced simultaneously with the flow.

# 4.3 Significance of inclination angle of the enclosure ( $\delta$ )

Technically, the inclination angle ( $\delta$ ) could be one of the vital constrain to be analysed. The nature of the problem involves an enclosure with heated left-curved and bottom walls and a cooler right-curved wall subjected to gravity



**Figure 6:** Flow pattern, isotherms, and local entropy generation for various inclination angles at Ra =  $10^5$ , Rd = 1,  $Q_0 = 5$ ,  $\gamma = 30^\circ$  and  $\phi = 0.02$ , and Ha = 20.

and magnetic forces from vertical and lateral sides, respectively. Figure 6 discloses the fact that a change in inclination angle ( $\delta$ ) significantly alters the movement, heat, and entropy aspects of the enclosure. Streamlines were clearly showing the alterations that ensued due to the inclination angle, which changes the phases of the flow. At  $\delta = 0$ , primary circulation fills the enclosure and moves in a clockwise manner with  $\psi_{\rm min}$  = -10.21, and looks active at the centre of the enclosure. As it tilted for increasing inclination angle  $\delta$  = 45° the swapping starts, and two flow circulations are observed. The upper vortices flow in a clockwise direction, while the lower vortices flow in an anticlockwise direction. Again, by increasing  $\delta = 90^{\circ}$ , the circulation inside the cavity is only in an anticlockwise direction with  $\psi_{\min}$ = 7.90. Thermal transference and an entropy loss of the system also get altered notably for inclination angle ( $\delta$ ) variations. The main factor behind this could be the sides switching during the rotation of the enclosure. Initially, the hotter side is sited at the left and bottom from which the vertical heat dissipation and entropy losses can be noted towards the cooler side. The enclosure tends to drift the sides in such a way that the hotter sides were at the bottom and right.

Lateral heat dissipation and entropy loss can be noted at the farther end of the enclosure.

# **4.4** Significance of angle of inclination of the magnetic field (γ)

Figure 7 displays that when the magnetic field inclines from 0° to 30° degrees, the crater is primarily filled with major vortices and the strength of the inferior vortices declines correspondingly. This indicates that as the inclination angle of the magnetic rises, the nature of the magnetic force alters, and the buoyancy force's effect is suppressed. When  $\gamma$  rises from 60° to 90°, visible recirculation zones are formed that reflect that there is a strong magnetic force to stabilize the buoyancy effect. It can be detected obviously via the figure that  $\psi_{\min}$  increases from -8.97 to -21.62 with an increment in  $\gamma$  from 0 to 0°. The concentration of isothermal lines along the cavity's heated walls indicates that the transmission manner of heat transmission predominates over convection. Since the magnetic force, also known

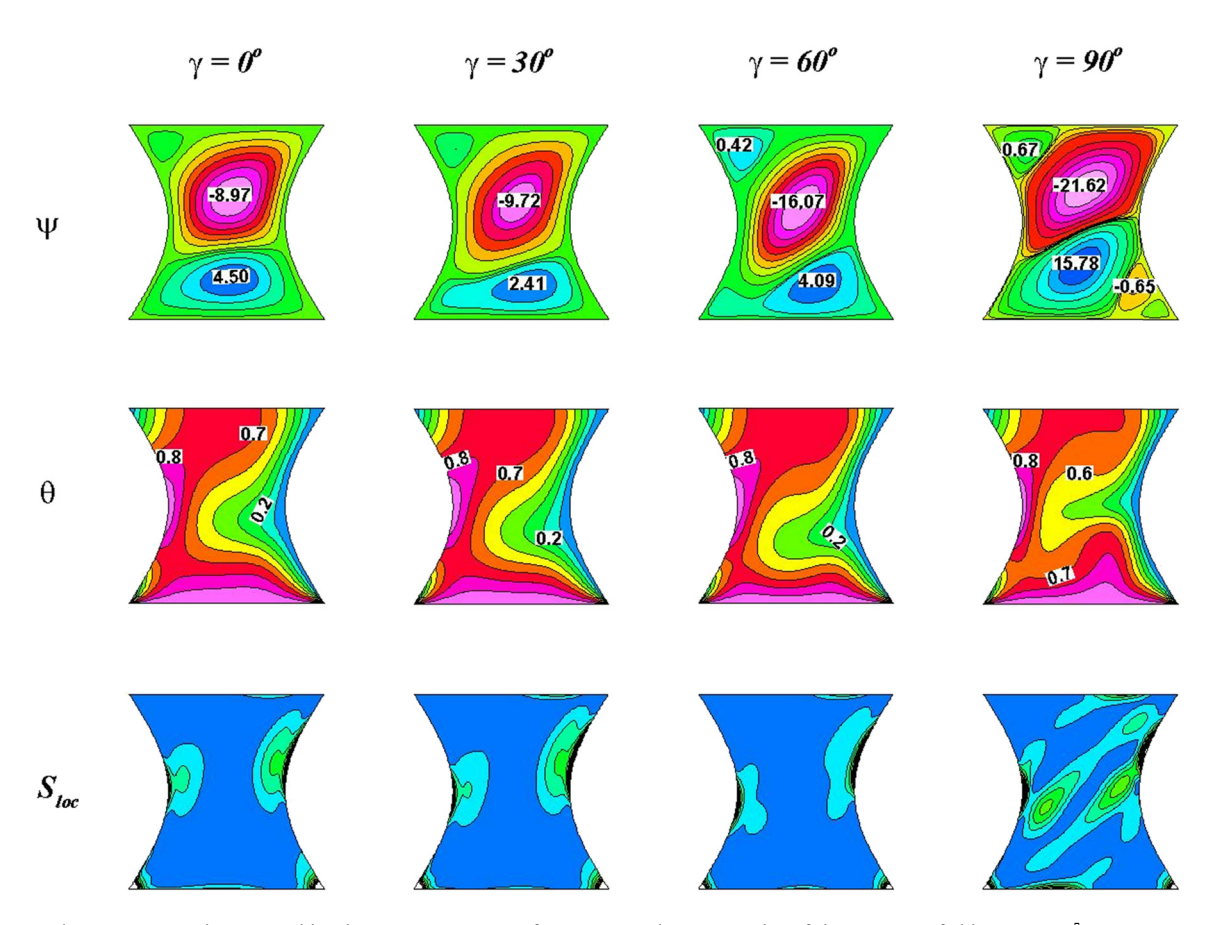


**Figure 7:** Flow pattern, isotherms, and local entropy generation for various inclination angles of the magnetic field at Ra =  $10^5$ , Rd = 1,  $Q_0 = 5$ ,  $\delta = 45^\circ$  and  $\phi = 0.02$ , and Ha = 20.

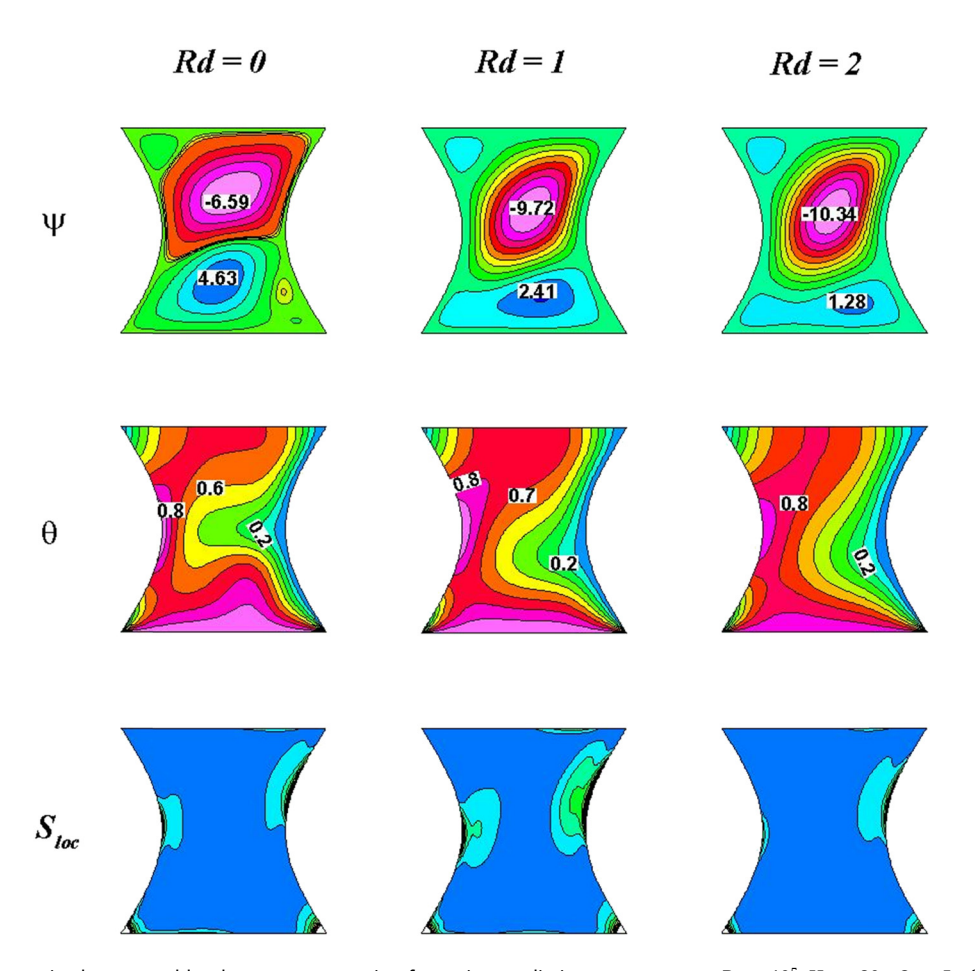


**Figure 8:** Flow pattern, isotherms, and local entropy generation for various radiation parameters at Ra =  $10^5$ , Ha = 20,  $Q_0 = 5$ ,  $\delta = 45^\circ$ ,  $\gamma = 30^\circ$ , and  $\phi = 0.02$ .

as the Lorentz force, increases in the inclined angle of the magnetic field, the fluid stratification inhibits the buoyancy effect. Entropy production rises with an increase in magnetic tilted angle as can be realized from the figure.

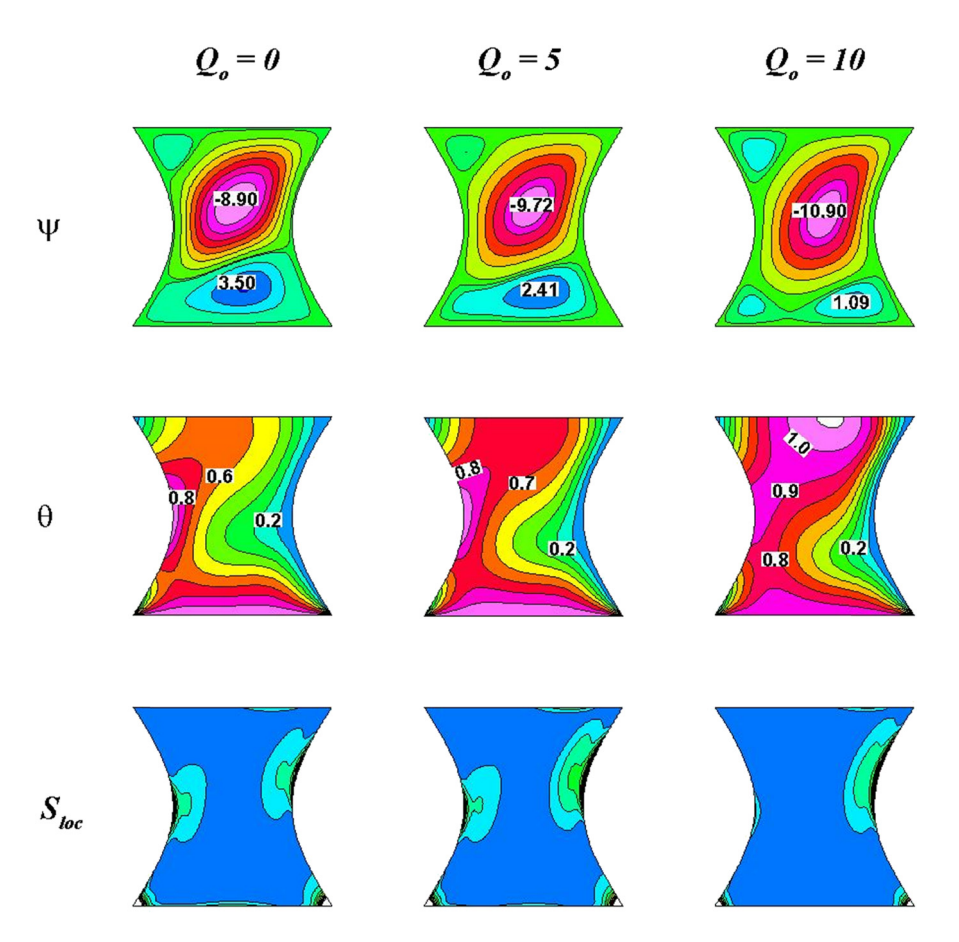
## 4.5 Significance of thermal radiation (Rd)

Figure 8 shows the variation of radiation parameters. As radiation number (Rd) values increase, the streamlines slightly increase within the enclosure. The secondary vortices near the enclosure bottom get reduced in size. The value  $\psi_{\rm min}$  increases from -6.59 to -10.34, while the value  $\psi_{\rm max}$  decreases from 4.63 to 1.24 with an increase in Rd from 0 to 2. The heat field shows that the density of the isotherms rises as the radiation parameter grows. Thermal radiation generally causes significant heat transfer from the heated side to the cold side. By strengthening the vortex and raising the buoyant force, the radiation parameter accelerates the fluid motion and raises the rate of heat transfer. Heat loss along walls occurs as a result of

the increase in temperature gradient that increases the entropy generation ( $S_{loc}$ ).

# 4.6 Significance of heat generation parameter $(Q_0)$

It is evident from Figure 9 that the heat generation parameter significantly affects the streamlines and isotherms. An increase in heat generation causes an increase in fluid temperature, and there is a noticeable improvement in the fluid flow's intensity. The value of  $\psi_{\min}$  is increased whenever a rise in  $Q_0$  from 0 to 10 is indicated. The temperature gradient inside the cavity grows as heat generation rises. The fluid's temperature rises as the value of  $Q_0$  rises, indicating that the boundary thermal layer generates energy. The isotherm contours show that most of the enclosure space is covered by cold fluid at  $Q_0 = 0$ . For  $Q_0 > 0$ , the fluid's temperature increases as a result of heat generation within the enclosure. The constricted area of the enclosure and its lower corners appear to have higher entropy loss than the rest of it.



**Figure 9:** Flow pattern, isotherms, and local entropy generation for various heat generation parameters at Ra =  $10^5$ , Ha = 20, Rd = 1,  $\delta = 45^\circ$ ,  $\gamma = 30^\circ$ , and  $\phi = 0.02$ .

#### 4.7 Significance of fractional volume

Figure 10 shows the disparities in streamlines, isotherms, and entropy generation with variation in nanoparticle volume fraction. The figure shows insignificant changes in the flow pattern although there is a growth in movement velocity due to the presence of solid nanoparticles. The isotherm pattern becomes linear with the rise in  $\phi$ ; this happens due to an increase in thermal conductivity that tends to intensify the temperature of the nanofluid. The incorporation of solid nanoparticles enhances the flow field's thermal conductivity, resulting in improved temperature distribution and less irreversibility during heat transfer across fluid layers. Respectively, the entropy loss seems to be more comparatively in the squeezed part of the enclosure and its bottom corners. The thermal conductivity of the nanofluid grows with increasing values of  $(\phi)$ , which causes an increase in the Nusselt number values.

#### 4.8 Thermal transference and entropy rate

A dimensionless parameter, or Nusselt number, is computed along the thermally heated wall of the cavity to better understand convective heat transfer phenomena. When the amounts of heat transfer and vortex velocity degrade, so does the overall entropy generation. This is widely understood to mean the configuration of heat transmission, entropy generation, magnetic field, and the movement of fluids. Figure 11 discloses the 2D graphical representation of the average Nusselt number (Nu<sub>avg</sub>) and the total entropy state concerning fractional volume  $(\phi)$ and Rayleigh number (Ra). The better thermal efficiency of the hybrid nano combination of fluid can be viewed for higher fractional volume which leads to a rise in entropy loss too. A rise in Rayleigh number (Ra) increases the density differences, and so amplifies flow convection excitation. Increasing the temperature differential between cold

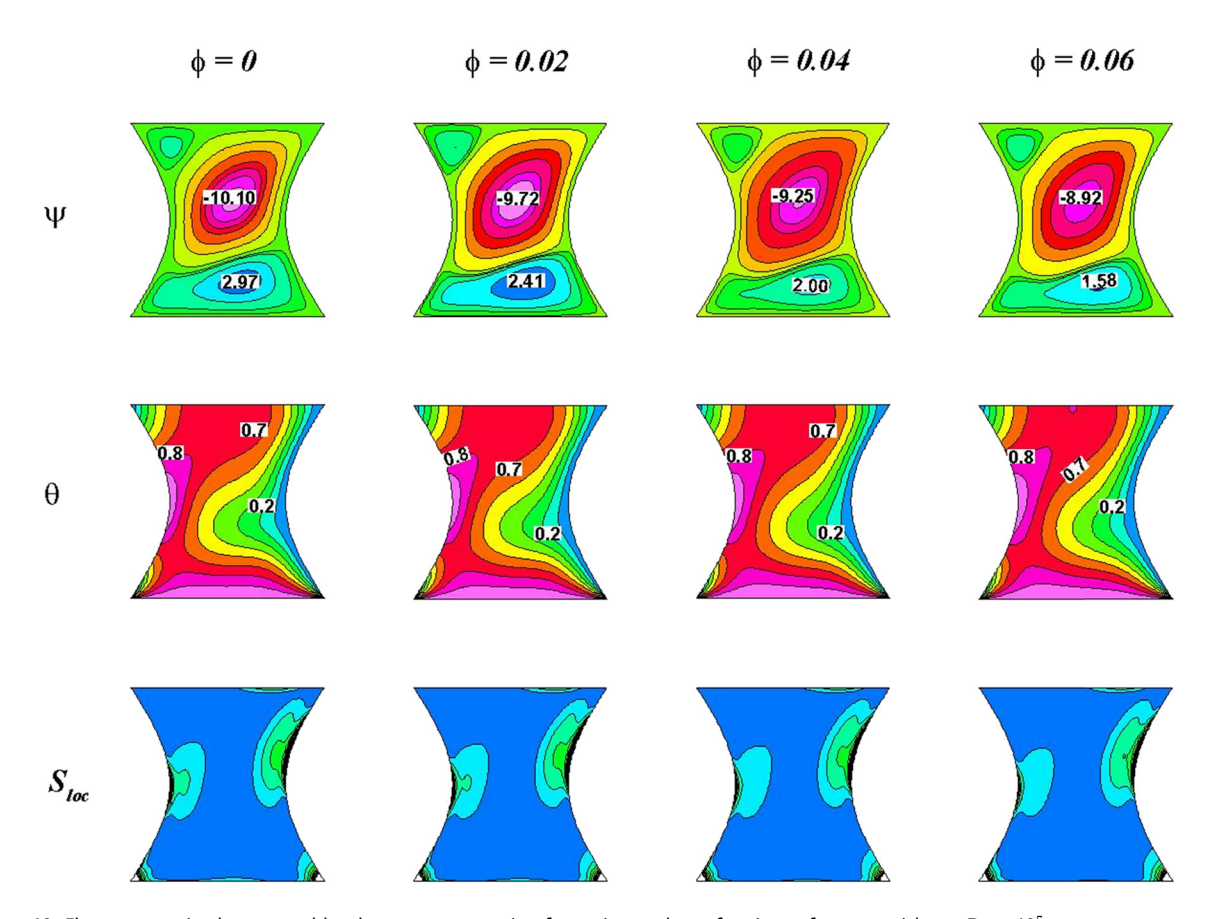
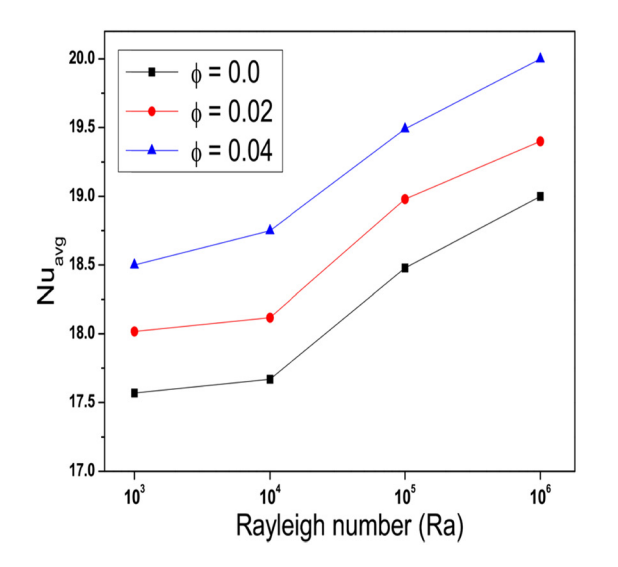


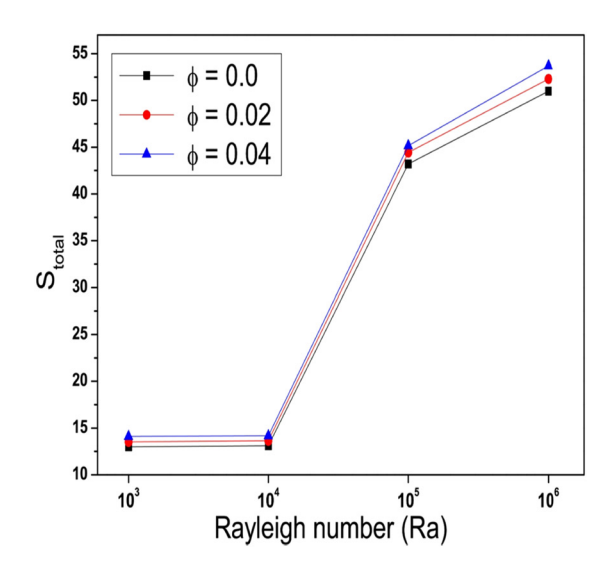
**Figure 10:** Flow pattern, isotherms, and local entropy generation for various volume fractions of nanoparticles at Ra =  $10^5$ , Rd = 1,  $Q_o$  = 5,  $\delta$  =  $45^\circ$ ,  $\gamma$  =  $30^\circ$ , and Ha = 20.

and hot sources will, however, boost the  $\ensuremath{\text{Nu}_{\text{avg}}}$  and entropy generation.

Figure 12 represents that the heat transport rate weakens with the rise in Ha. The influence of Lorentz force decreases

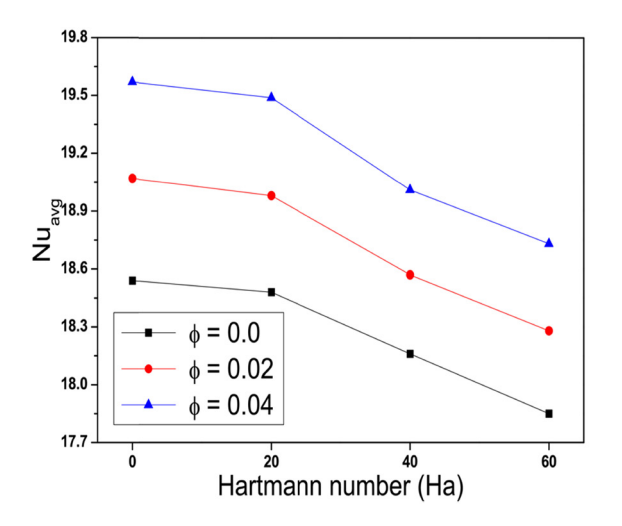
the fluid flow velocity, and hence, the average Nusselt number also decreases. The entropy generation also decreases due to the presence of resistive force caused by the magnetic field. 2D representations in Figure 13 illustrate the impact of cavity





**Figure 11:** Total entropy generation ( $S_{\text{total}}$ ) and mean Nusselt number (Nu<sub>avg</sub>) for various Rayleigh numbers (Ra) at Rd = 1,  $Q_0$  = 5,  $\delta$  = 45°,  $\gamma$  = 30°, and Ha = 20.

14 — Syed M. Hussain et al. DE GRUYTER



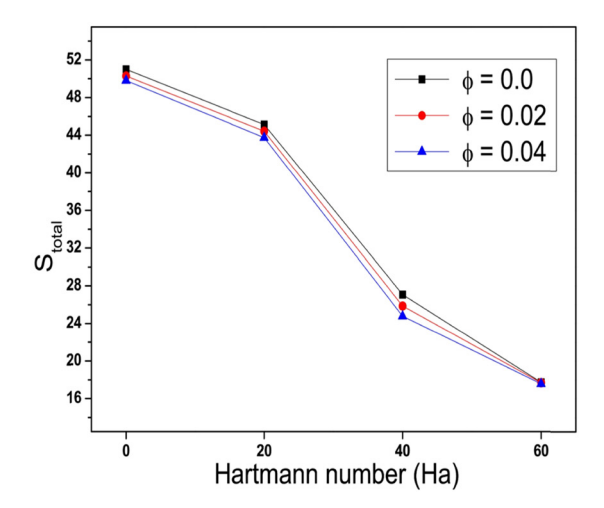


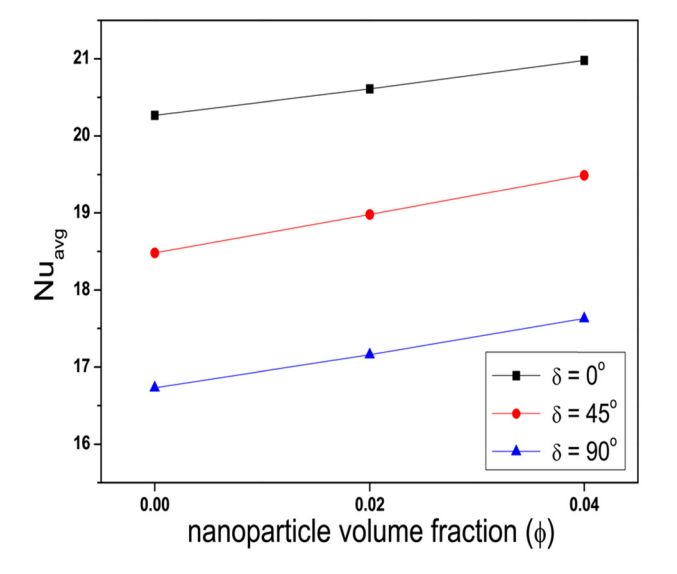
**Figure 12:** Total entropy generation ( $S_{\text{total}}$ ) and mean Nusselt number ( $Nu_{\text{avg}}$ ) for dissimilar Hartmann numbers (Ha) at Ra =  $10^5$ , Rd = 1,  $Q_0$  = 5,  $\delta$  =  $45^\circ$ , and  $\gamma$  =  $30^\circ$ .

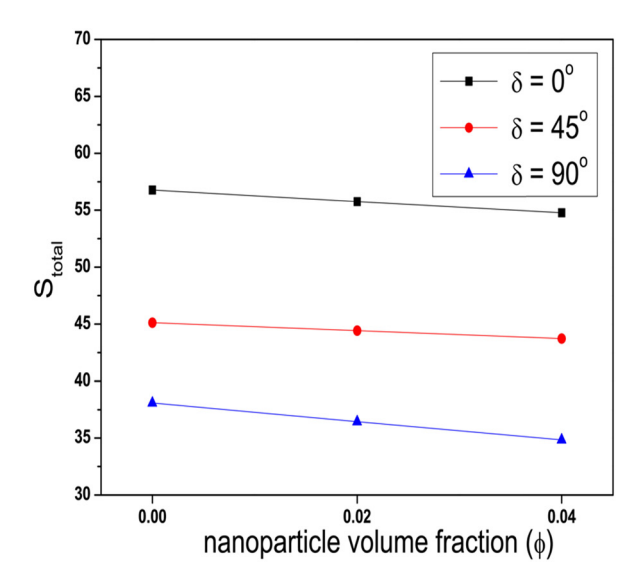
inclination angle over the mean Nusselt number (Nu<sub>avg</sub>) and the entropy formation rate. In terms of inclination angle ( $\delta$ ), the trends get reversed to work against it. In particular, the entropy formation drops significantly at the earlier alteration of the inclination angle ( $\delta$ ) due to phase changing process of the enclosure when compared to its higher alterations where the changes get settled into another form.

Figure 14 displays the difference between the Nusselt number and entropy production for the inclined angle of the magnetic field. Accumulative the magnetic field liking angle (y) enhances the convective temperature transmission presentation. With an increase in y rate, the current resistance gets minor close to the warm lower wall, and

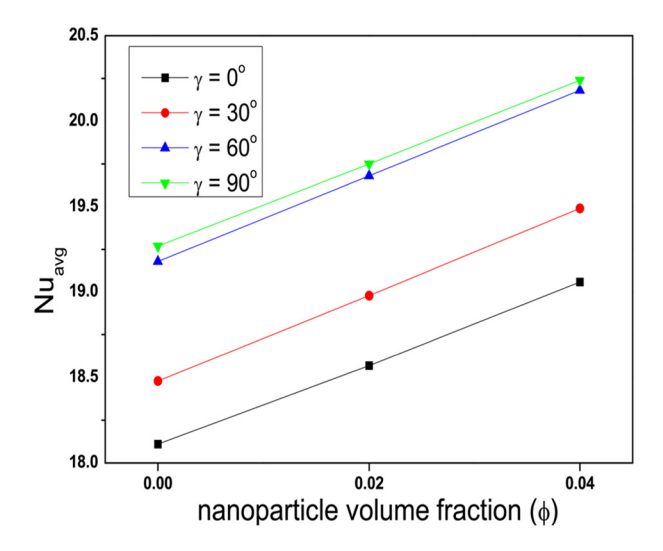
consequently, the magnetic force rises the thermal diffusion procedure utilizing the conduction development. The total entropy generation also drops with an increase in magnetic inclination angle.

From Figure 15, the consistent rise in thermal dispersal rate for higher thermal radiation can be noted. This may be because additive heat is available in the system, which encounters the better heat transfer fluid. In terms of entropy formation, the radiation acts in dual ways. Initially, it tends to rise and reach a peak value, and then, the entropy loss gets dropped. The reason behind such behaviour could be the thermally saturated stage of the enclosure after being exposed to such radiation heat to some extent.





**Figure 13:** Total entropy generation ( $S_{\text{total}}$ ) and mean Nusselt number ( $Nu_{\text{avg}}$ ) for various inclination angles of the cavity ( $\delta$ ) at Ra = 10<sup>5</sup>, Rd = 1,  $Q_0$  = 5,  $\gamma$  = 30°, and Ha = 20.



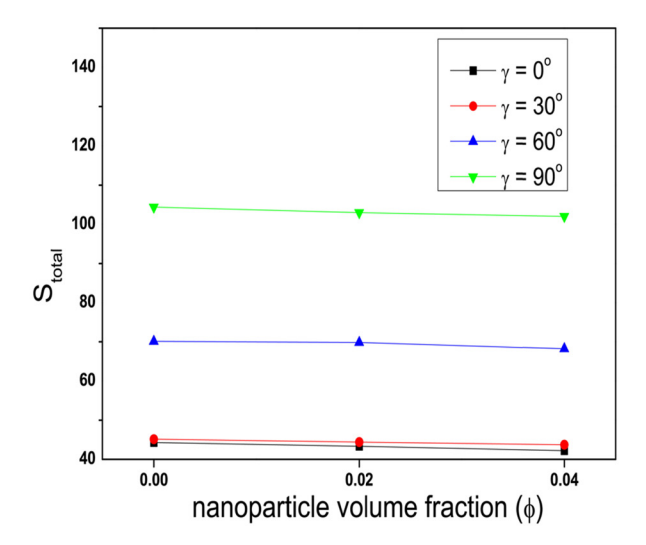
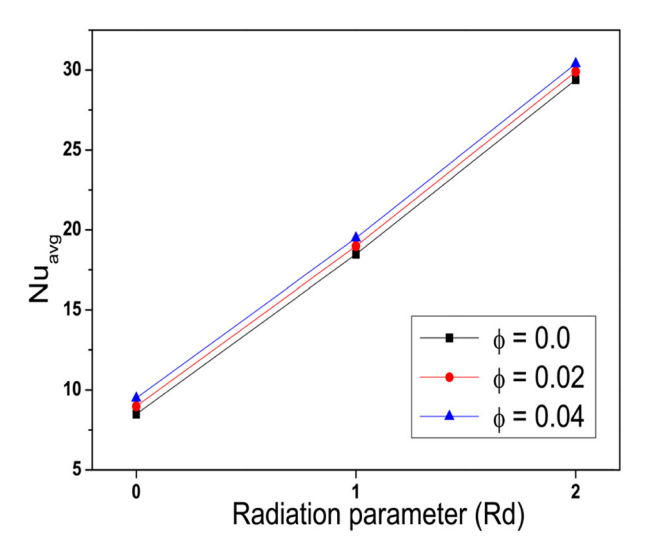


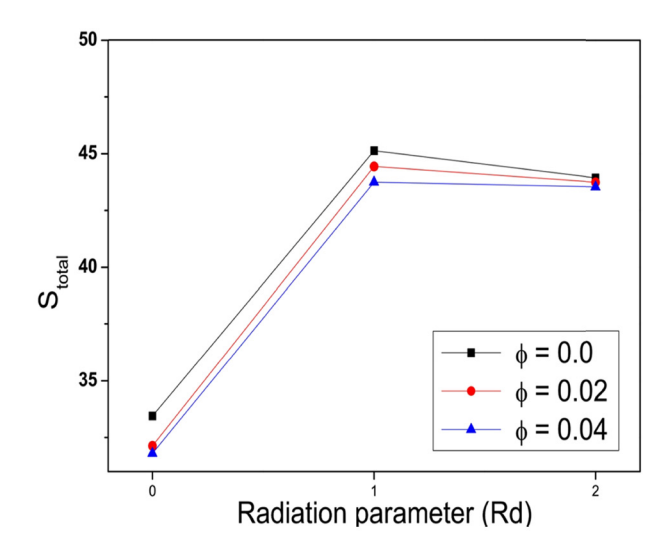
Figure 14: Total entropy generation ( $S_{total}$ ) and mean Nusselt number ( $Nu_{avg}$ ) for various inclination angles of the magnetic field (y) at  $Ra = 10^5$ , Rd = 1,  $Q_0 = 5$ ,  $\delta = 45^\circ$ , and Ha = 20.

Figure 16 shows that the heat transfer rate augments by augmenting the heat generation parameter. At  $Q_0 = 0$ , the maximum heat transfer rate is realized. Nevertheless, as  $Q_0$  rises, the heat starts generating inside the cavity, which enhances the temperature and therefore reduces the current gradients in the enclosure. This results in a decrease in heat transfer rate as  $Q_0$  is increased. Minimal heat transfer rate is gained for  $Q_0 = 10$  by entirely the nanoparticle amounts. The total entropy generation augments with a rise in the heat generation parameter.

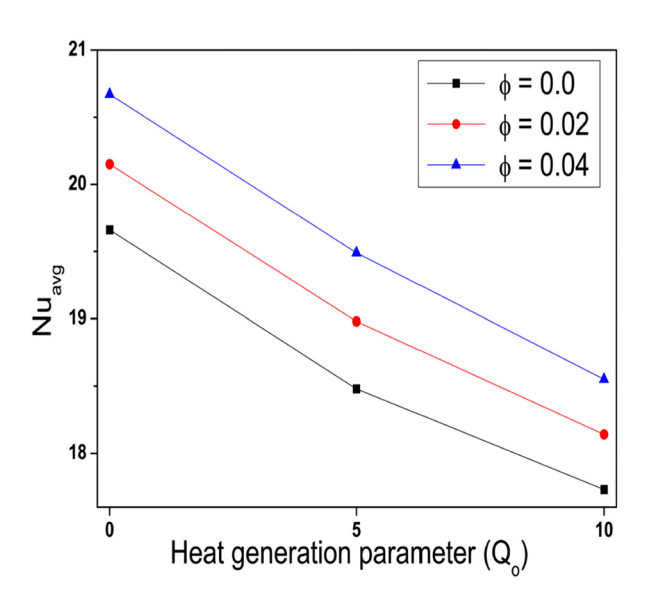
#### 5 Conclusion

In this study, irreversible energy loss and the thermal dispersal using hybrid fluid flow over a squeeze enclosure subjected to magnetic and radiative heating were made with the outer inner iteration procedure, and BiCGStab was performed. The enclosure's left and bottom walls of the enclosure were hotter, and the right wall was assumed to be cold as the top wall set adiabatic. A finite difference approach is employed to solve the governing dimensionless equations of





**Figure 15:** Total entropy generation ( $S_{\text{total}}$ ) and mean Nusselt number ( $Nu_{\text{avg}}$ ) for dissimilar radiation parameters (Rd) Ra =  $10^5$ , Ha = 20,  $Q_0 = 5$ ,  $\delta = 45^\circ$ , and  $\gamma = 30^\circ$ .



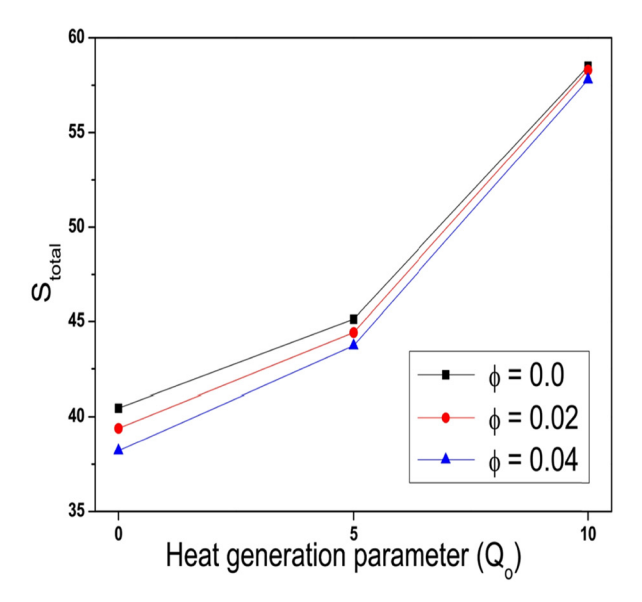


**Figure 16:** Total entropy generation ( $S_{\text{total}}$ ) and mean Nusselt number ( $Nu_{\text{avg}}$ ) for various heat generation parameters ( $Q_0$ ) Ra =  $10^5$ , Ha = 20, Rd = 1,  $\delta$  =  $45^\circ$ , and  $\gamma$  =  $30^\circ$ .

conservation in vorticity form. Verification of the numerical scheme engaged in this work was performed through the comparative analysis. Based on the validation, the results for entropy and thermal aspects were obtained and displayed as entropy loss, streamlines, Nusselt number, and isotherms. The following inference was collectively acquired:

- Rayleigh number (Ra) changes induce convection effect in an enclosure, which works in favour of heat transference and simultaneously the energy loss also on the higher side. The heat transfer rate and entropy production are increased by growing Ra.
- Fractional volume ( $\phi$ ) reflects the heat transference strength of the flowing fluid, which assists thermal dispersal in the enclosure along with the entropy.
- A stronger magnetic field has a refractory effect, which slows down the flow velocity. The flow and heat transfer abilities are found to be much greater without any sort of magnetic force (Ha = 0). As Ha rises, convection within the cage reduces down and conduction takes over.
- Significant changes in flow patterns and thermal distribution patterns are observed when the geometric inclination angle changes correspond with the direction of gravity. The convection strength varies with a change in geometric tilt angle. Maximum thermal energy dissipation and entropy generation is observed at  $\delta = 90^{\circ}$ .
- The amount of heat dissipation within the enclosure decreases as the heat generation parameter (Q) increases because of the modification in the current gradient produced by inner heat generation. An improvement in  $Q_0$  from 0 to 10 hints to a reduction in the heat transfer amount for convection-dominant suitcases.

- A change in the magnetic force (Lorentz) caused by a rise in the inclined angle of the magnetic field (y) accelerates fluid wave and heat conduction or diffusion via convection.
- Radiation heat (Rd) adds more load in the heat transfer process, while it tends to drive away such incoming heat from the radiating source.

From the present study, we can conclude that the buoyancy effect (due to Ra), heat generation, and thermal radiative flux serve as a good heat and fluid flow regulator inside the cavity, and optimal heat transfer rates can be achieved by careful selection of these parameters.

Practical applications for the results of this study of  $Ag-TiO_2-H_2O$  combination fluid convective movement issues inside a motivated geometry through interior heat generation and thermal radiation include nuclear reactors, geophysics, solar energy to heat conversion, cooling electronic equipment, and others.

## **6 Future directions**

The accomplished research work can be further studied in the future by considering the implications of Hall current, induced magnetic field, viscous, and Joule dissipations.

**Acknowledgments:** The authors extend their appreciation to the Deanship of Research and Graduate Studies at King Khalid University for funding this work through Large Research Project under Grant Number RGP2/360/45.

**Funding information:** This research was funded by the Deanship of Research and Graduate Studies at King Khalid University through Large Research Project under Grant Number RGP2/360/45.

**Author contributions:** All authors have accepted responsibility for the entire content of this manuscript and approved its submission.

**Conflict of interest:** The authors state no conflict of interest.

## References

- [1] Choi, S. U. and J. A. Eastman. Enhancing thermal conductivity of fluids with nanoparticles (No. ANL/MSD/CP-84938; CONF-951135-29), Argonne National Lab, IL (United States), 1995.
- [2] Tiwari, R. K. and M. K. Das. Heat transfer augmentation in a twosided lid-driven differentially heated square cavity utilizing nanofluids. *International Journal of Heat and Mass Transfer*, Vol. 50, No. 9–10, 2007, pp. 2002–2018.
- [3] Buongiorno, J. Convective transport in nanofluids. *Journal of Heat Transfer*, Vol. 128, No. 3, 2006, pp. 240–250.
- [4] Abderrahmane, A., W. Jamshed, A. M. Abed, G. F. Smaisim, K. Guedri, S. Suriya Uma Devi, et al. Heat and mass transfer analysis of non-Newtonian power-law nanofluid confined within annulus enclosure using Darcy-Brinkman-Forchheimer model. *Case Studies in Thermal Engineering*, Vol. 40, 2022, id. 102569.
- [5] Alam, Md. S., S. S. Keya, U. Salma, S. M. Chapal Hossain, and Md. M. Billah. Convective heat transfer enhancement in a quarter-circular enclosure utilizing nanofluids under the influence of periodic magnetic field. *International Journal of Thermofluids*, Vol. 16, 2022, id. 100250.
- [6] Shuvo, Md. S., M. H. Hasib, and S. Saha. Entropy generation and characteristics of mixed convection in lid-driven trapezoidal tilted enclosure filled with nanofluid. *Heliyon*, Vol. 8, 2022, id. e12079.
- [7] Yeasmin, S., M. M. Billah, Md. Z. Molla, and K. E. Hoque. Numerical analysis of unsteady mixed convection heat transfer characteristics of nanofluids confined within a porous lid-driven L-shaped cavity. *International Journal of Thermofluids*, Vol. 16, 2022, id. 100218.
- [8] Heidarshenas, A., Z. Azizi, S. M. Peyghambarzadeh, and S. Sayyahi. Experimental investigation of heat transfer enhancement using ionic liquid-Al<sub>2</sub>O<sub>3</sub> hybrid nanofluid in a cylindrical microchannel heat sink. Applied Thermal Engineering, Vol. 191, 2021, id. 116879.
- [9] Kanti, P. K., K. V. Sharma, Z. Said, and M. Gupta. Experimental investigation on thermo-hydraulic performance of water-based fly ash–Cu hybrid nanofluid flow in a pipe at various inlet fluid temperatures. *International Communications in Heat and Mass Transfer*, Vol. 124, No. April, 2021, id. 105238.
- [10] Acharya, N. Magnetized hybrid nanofluid flow within a cube fitted with circular cylinder and its different thermal boundary conditions. *Journal of Magnetism and Magnetic Materials*, Vol. 564, 2022, id. 170167.
- [11] Acharya, N. and H. F. Oztop. On the entropy analysis and hydrothermal behavior of buoyancy-driven magnetized hybrid nanofluid flow within a semi-circular chamber fitted with a triangular heater:

- Application to thermal energy storage for energy management. *Numerical Heat Transfer, Part A: Applications*, 2023.
- [12] Nayak, M. K., N. Karimi, A. J. Chamkha, A. S. Dogonchi, S. El-Sapa, and A. M. Galal. Efficacy of diverse structures of wavy baffles on heat transfer amplification of double-diffusive natural convection inside a C-shaped enclosure filled with hybrid nanofluid. Sustainable Energy Technologies and Assessments, Vol. 52, No. Part B, 2022. id. 102180.
- [13] Al-Kouz, W., A. Abderrahmane, M. Shamshuddin, O. Younis, S. Mohammed, O. A. Bég, et al. Heat transfer and entropy generation analysis of water-Fe<sub>3</sub>O<sub>4</sub>/CNT hybrid magnetic nanofluid flow in a trapezoidal wavy enclosure containing porous media with the Galerkin finite element method. *The European Physical Journal Plus*, Vol. 136, 2021, id. 1184.
- [14] Ahmed, A. M., M. D. Shamshuddin, M. Ferdows, and M. R. Eid. Heat and mass transport through biaxial extending sheet with anisotropic slip and entropy/Bejan on the three-dimensional boundary layer hybrid nanofluid. *Proceedings of the Institution of Mechanical Engineers*, Part E: Journal of Process Mechanical Engineering, 2022.
- [15] Zhang, L., C. Chen, and Y.-R. Li. Coupled natural convection heat transfer inside and outside a closed cylindrical cavity with a uniform temperature heat source. Case Studies in Thermal Engineering, Vol. 52, 2023, id. 103659.
- [16] Hosseinzadeh, K. H., M. Roshani, M. A. Attar, D. D. Ganji, and M. B. Shafii. Heat transfer study and optimization of nanofluid triangular cavity with a pentagonal barrier by finite element approach and RSM. *Heliyon*, Vol. 9, 2023, id. e20193.
- [17] Sudarsana Reddy, P., P. Sreedevi, and V. Nageswara Reddy. Entropy generation and heat transfer analysis of magnetic nanofluid flow inside a square cavity filled with carbon nanotubes, chemical thermodynamics and thermal. *Analysis*, Vol. 6, 2022, id. 100045.
- [18] Roshani, H., P. Jalili, B. Jalili, I. Ahmad, A. S. Hendy, M. R. Ali, et al. The effect of magnetic field on the heat transfer in the porous medium octagonal cavity with Cassini oval barriers. *Case studies in Thermal Engineering*, Vol. 56, 2024, id. 104194.
- [19] Salawu, S. O., E. I. Akinola, and M. D. Shamshuddin. Entropy generation and current density of tangent hyperbolic Cu-C2H6O2 and ZrO<sub>2</sub>-Cu/C<sub>2</sub>H<sub>6</sub>O<sub>2</sub> hybridized electromagnetic nanofluid: A thermal power application. South African Journal of Chemical Engineering, Vol. 46, 2023, pp. 1–11.
- [20] Ahmed, S., A. Hossain, Md. Z. Hossain, and Md. M. Molla. Forced convection of non-Newtonian nanofluid in a sinusoidal wavy channel with response surface analysis and sensitivity test. *Results in Engineering*, Vol. 19, 2023, id. 101360.
- [21] Hossain, A. and M. M. Molla. MHD mixed convection of non-Newtonian power-law ferrofluid in a wavy enclosure. *Journal of Thermal Analysis and Calorimetry*, Vol. 148, 2023, pp. 11871–11892.
- [22] Afsana, S., M. M. Molla, P. Nag, L. K. Saha, and S. Siddiqa. MHD natural convection and entropy generation of non-Newtonian ferrofluid in a wavy enclosure. *International Journal of Mechanical Sciences*, Vol. 198, 2021, id. 106350.
- [23] Nag, P. and M. M. Molla. Double diffusive natural convection of non-Newtonian nanofluid considering thermal dispersion of nanoparticles in a vertical wavy enclosure. AIP Advances, Vol. 11, 2021. id. 095219.
- [24] Nabwey, H. A., A. M. Rashad, W. A. Khan, and S. I. Alshber. Effectiveness of magnetize flow on nanofluid *via* unsteady natural convection inside an inclined U-shaped cavity with discrete

- heating. *Alexandria Engineering Journal*, Vol. 61, No. 11, 2022, pp. 8653–8666.
- [25] Keerthi Reddy, N., H. A. Kumara Swamy, M. Sankar, and B. Jang. MHD convective flow of Ag-TiO2 hybrid nanofluid in an inclined porous annulus with internal heat generation. *Case studies in Thermal Engineering*, Vol. 42, 2023, id. 102719.
- [26] Moolya, S. and A. Satheesh. Role of magnetic field and cavity inclination on double diffusive mixed convection in rectangular enclosed domain. *International Communications in Heat and Mass Transfer*, Vol. 118, 2020, id. 104814.
- [27] Bakar, S. A., N. Md. Arifin, N. Bachok, and F. Md. Ali. Effect of thermal radiation and MHD on hybrid Ag-TiO2/H2O nanofluid past a permeable porous medium with heat generation. *Case Studies in thermal Engineering*, Vol. 28, 2021, id. 101681.
- [28] Algehyne, E. A., F. M. Alamrani, A. Khan, K. A. Khan, S. A. Lone, and A. Saeed. On thermal distribution of MHD mixed convective flow of a Casson hybrid nanofluid over an exponentially stretching surface with impact of chemical reaction and ohmic heating. *Colloid and Polymer Science*, Vol. 302, 2024, pp. 503–516.
- [29] Yasmin, H., S. Lone, F. Ali, H. Alrabaiah, Z. Raizah, and A. Saeed. Thermal radiative flow of cross nanofluid due to a stretched cylinder containing microorganisms. *Nanotechnology Reviews*, Vol. 12, No. 1, 2023, id. 20230147.
- [30] Yasmin, H., H. Hejazi, S. Lone, Z. Raizah, and A. Saeed. Time-independent three-dimensional flow of a water-based hybrid nanofluid past a Riga plate with slips and convective conditions: A homotopic solution. *Nanotechnology Reviews*, Vol. 12, No. 1, 2023, id. 20230183.
- [31] Aghakhani, S., A. H. Pordanjani, M. Afrand, M. Sharifpur, and J. P. Meyer. Natural convective heat transfer and entropy generation of alumina/water nanofluid in a tilted enclosure with an elliptic constant temperature: Applying magnetic field and radiation effects. *International Journal of Mechanical Sciences*, Vol. 174, 2020, id. 105470.
- [32] Mohammadi, M. and S. A. Gandjalikhan Nassab. Double-diffusive convection flow with Soret and Dufour effects in an irregular

- geometry in the presence of thermal radiation. *International Communications in Heat and Mass Transfer*, Vol. 134, 2022, id. 106026.
- [33] Yu, Q., H. Xu, and S. Liao. Analysis of mixed convection flow in an inclined lid-driven enclosure with Buongiorno's nanofluid model. *International Journal of Heat and Mass Transfer*, 2018.
- [34] Ahmed, S. A., P. B. A. Reddy, S. Jakeer, A. M. Rashad, and T. Salah. Magnetic convection-radiation interaction in wavy porous triangular containers using hybrid nanofluid: Entropy analysis. *Journal* of Porous Media, Vol. 26, No. 5, 2023, pp. 79–99.
- [35] Afrand, M., A. H. Pordanjani, S. Aghakhani, H. F. Öztop, and N. Abu-Hamdeh. Free convection and entropy generation of a nanofluid in a tilted triangular cavity exposed to a magnetic field with sinusoidal wall temperature distribution considering radiation effects. *International Communications in Heat and Mass Transfer*, Vol. 112, 2020. id. 104507
- [36] Biswal, P. and T. Basak. Entropy generation based approach on natural convection in enclosures with concave/convex side walls. *International Journal of Heat and Mass Transfer*, Vol. 82, 2015, pp. 213–235.
- [37] Parveen, R., T. R. Mahapatra, and B. C. Saha. Study of entropy generation and MHD natural convection in a curved enclosure having various amplitude and filled with Cu–TiO<sub>2</sub>/water hybrid nanofluid. *Journal of Nanofluids*, Vol. 10, No. 3, 2021, pp. 339–354.
- [38] Parveen, R. and T. R. Mahapatra. Heat and mass source effect on MHD double-diffusive mixed convection and entropy generation in a curved enclosure filled with nanofluid. *Nonlinear Analysis: Modelling and Control*, Vol. 27, No. 2, 2022, pp. 308–330.
- [39] Ece, M. C. and E. Büyük. Natural convection flows under a magnetic field in an inclined rectangular enclosure heated and cooled on adjacent walls. *Fluid Dynamics Research*, Vol. 38, No. 8, 2006, pp. 564–590.
- [40] Roy, S. and T. Basak. Finite element analysis of natural convection flows in a square cavity with non-uniformly heated wall(s). *International Journal of Engineering Science*, Vol. 43, 2005, pp. 668–680.